

# EFFECTS OF VARIOUS THIN FILM COATING TECHNIQUES ON POOL BOILING HEAT TRANSFER

**Gwang Hyeok Seo, Hong Hyun Son, Uiju Jeong, Gyoodong Jeun, and Sung Joong Kim\***

Department of Nuclear Engineering, Hanyang University  
222 Wangsimni-ro, Seongdong-gu, Seoul, 133-791, Republic of Korea  
seokh3@hanyang.ac.kr; hhson@hanyang.ac.kr; ujjeong@hanyang.ac.kr;  
thlab@hanyang.ac.kr; sungjkim@hanyang.ac.kr

## ABSTRACT

To investigate the effects of thin film, chromium (Cr) and carbon nanotube (CNT) films were fabricated on a stainless steel grade 316 (SS316) substrate. The Cr coated heaters was produced via a sputtering process. The sputtering powers and times were carefully controlled to produce well-defined Cr layers on the substrate. On the other hand, CNT coated heaters were produced through a vacuum filtration processes. After preparing the test heaters, the coating surface was characterized using various measurements. The surface wettability was quantified by the measurement of contact angles. The surface morphology was examined by scanning electron microscopy (SEM). The contact angle measurement shows a great increase in wettability for a Cr coated heater while the wettability of the CNT coated heater decreases slightly. Moreover, the SEM images indicate that the Cr structures were compactly distributed showing nanoscale cavities. The experimental results of pool boiling tests show that, although a great increase in wettability was evaluated after the sputtering process, no enhancement of CHF was observed for the Cr coated heater. However, though the surface wettability and roughness decreased slightly, the porous structure of CNT arrays significantly enhanced the CHF.

## KEYWORDS

sputtering, carbon nanotube, thin film, critical heat flux, nucleate boiling heat transfer coefficient

## 1. INTRODUCTION

Over the past few decades, nuclear power has been paid attention for its high power density and stable supply. Although a few severe accidents occurred and resulted in exceeding consequences to the environment and the public, noticeable progress have also been made for the nuclear safety. After the accident at Three Mile Island in 1980s, the importance of a probabilistic approach for the risk analysis was recognized more seriously. Also, passive safety systems were considerably developed, and currently introduced to several reactor types, which are the Westinghouse's AP1000 and South Korea's OPR1000 to mention a few [1]. Furthermore, since the Fukushima Daiich accident in 2011, various strategies were suggested and envisioned for severe accident mitigation and enhancement of safety margin [2, 3]. For example, reactor cavity flooding, which is a kind of in-vessel retention (IVR) strategies, is envisioned to prevent the RPV failure against the hypothesized melting of reactor core [4, 5]. In addition to the severe accident mitigation strategies, the development of accident tolerant fuels (ATFs) has received attention for

the improved safety of a nuclear reactor system. With an introduction of ATF system, minimized cladding oxidation and retention capability of fission products could be achieved [1].

In order to attain the improved safety with the suggested strategies, a coating technique for surface modification is capable of a solution. Since critical heat flux (CHF) is often considered as a limit criterion for a thermal system, appropriate thermal management is important in adopting the strategies mentioned. The delayed RPV failure is expected with proper introduction of the cooling outside the RPV and enhanced CHF on the RPV surface. As many studies reported, the CHF enhancement is observed on an engineered surface, and this can be achieved using a surface coating technique. Furthermore, the adoption of coating techniques is one of promising approaches for ATF systems because surface modification with a highly oxidation-resistant material can prevent hydrogen generation and cladding embrittlement [1].

Compared to the development of a new cladding for the replacement of the current zirconium-based alloy cladding and new fuel forms instead of the current ceramic oxide fuels, the surface coating technique is cost-effective and easily applicable to the current LWR system with no significant design changes.

Recently, a wide variety of oxidation-resistant materials have been proposed: iron-based alloys and SiC-based materials [6]. Among them, chromium (Cr) is suggested as a coating material for fuel claddings because it is known for has oxidation-resistant characteristic.

In this study, the feasibility of different coating techniques was investigated in terms of boiling heat transfer and CHF. Chromium (Cr) and carbon nanotube (CNT) films were fabricated on a metal substrate via a physical vapor deposition (PVD) and vacuum filtration processes. After preparing test specimens, pool boiling heat transfer experiments were carried out to investigate the boiling performance of both cases.

## 2. EXPERIMENTAL

### 2.1. Sputtering Process to Generate Cr Film

Cr film was deposited using a DC sputtering system. Figure 1 shows a schematic of the sputtering system. A metal target is placed in a downward direction in the upper region of the vacuum chamber, and a substrate facing the target is positioned at the bottom region. The substrate and the target are 100 mm apart from each other. The size of the target is 101.6 x 6.35 mm<sup>2</sup> in diameter and thickness, respectively. Purity of the Cr target is 99.95%. The DC power supply provides up to 1000 W, and the substrate stage can be heated to a maximum temperature of 600 °C.

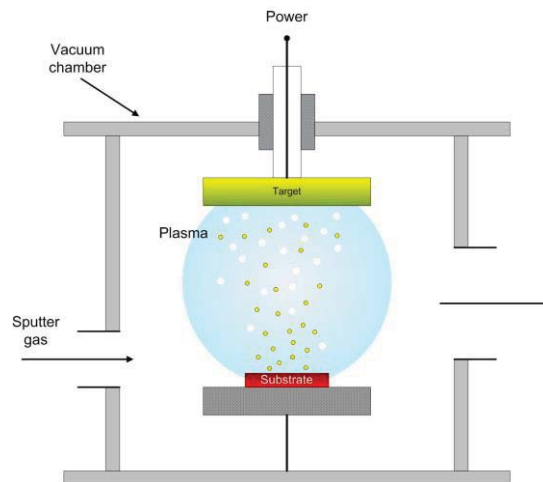
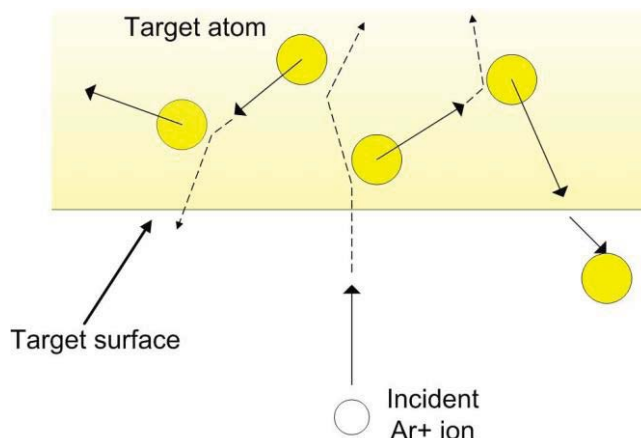


Figure 1. Sputter deposition system.

Once a sputtering process begins, the chamber is evacuated to a base pressure of  $2 \times 10^{-3}$  Pa. Argon (Ar) sputter gas flows to the chamber, and the chamber pressure is maintained at a specific condition. Before starting Cr deposition, the target is sputtered by  $\text{Ar}^+$  ions for 5 min to remove any contaminants on the surface. After the surface cleaning, the target is bombarded with the energetic  $\text{Ar}^+$  ions to generate sputter atoms from the target surface as described schematically in Fig. 2. During the PVD process described, the sputtering conditions are carefully kept to produce a desirable film on the substrate, and the conditions are summarized in Table I.



**Figure 2. Physical sputtering process.**

**Table I. Summary of sputtering conditions**

Target	Flow rate, cc	Sputtering power, W	Sputtering time, hr	Pressure, Pa
Cr	30	150	2	0.13

## 2.2. Fabrication of Random CNT Network Film

CNTs were dispersed in deionized water with 2 wt % sodium dodecyl sulfate (SDS) or sodium cholate. The prepared solution was homogenized at 6500 rpm for one hour and sonicated for 10 minutes in a cup-horn sonicator. The diameter and length of CNTs were approximately 0.8 – 1.2 nm and 0.1 – 1.4  $\mu\text{m}$ , respectively, although the individual lengths may have varied depending on the sonication time. The density-gradient ultracentrifugation was used to separate CNTs by the subtle difference of densities at 30,000 rpm, and the upper portion of the solution in well-dispersed solution was only decanted (Fig. 3(a)) [7]. A randomly oriented CNT film was fabricated by a vacuum filtration method [8]. The CNT solution was filtered through a porous alumina membrane (Anodisc 25 mm in diameter, 20 nm to 100 nm in pore size) to fabricate a randomly oriented CNT network film (Fig. 3(b)). The total amount of CNT solution was generally proportional to the thickness of the synthesized film according to the characterizations by an atomic force microscope (AFM), and it allowed us to control the thickness of the CNT film. The remaining surfactants were removed by repetitive washing by DI water until no bubbles were observed through the vacuum filtration equipment, and the final CNT film on the alumina-supported membrane was obtained (Fig. 3(c)).



**Figure 3. (a) Dispersed HiPco CNT solutions; (b) Vacuum filtration equipment for the synthesis of randomly oriented CNT network film; (c) CNT film with a supporting substrate.**

The alumina membrane that was covered with a CNT film was floated on a 3 M sodium hydroxide (NaOH) solution to induce the gradual etching of the bottom layer of the membrane [9]. When the entire alumina layer was etched, the remaining CNT film floated on NaOH solution. A repetitive DI water circulation reduced most of sodium hydroxide until pH 7 was reached, where the free-standing CNT film floated on the DI water surface. The test heater was placed directly underneath the CNT film, and the DI water was continuously drained until physical adhesion of the film to the test heater occurred. The CNT film was transferred onto the center of the test heater, and the CNT coated heater was bolted to the copper electrodes before being insulated with epoxy. Incomplete removal of DI water between the CNT film and the test heater resulted in weaker adhesion. The CNT coated test heater was dried in an oven at 80 °C for 2 hours to promote adhesion. The thickness of the CNT film was precisely measured by AFM near the boundary between the CNT film and its substrate (Fig. 4(a)). Figure 4(b) shows the surface morphology of randomly oriented CNT networks, captured by a scanning electron microscope (SEM). The random fiber networks composed of CNTs were well distributed with uniform porous structures.

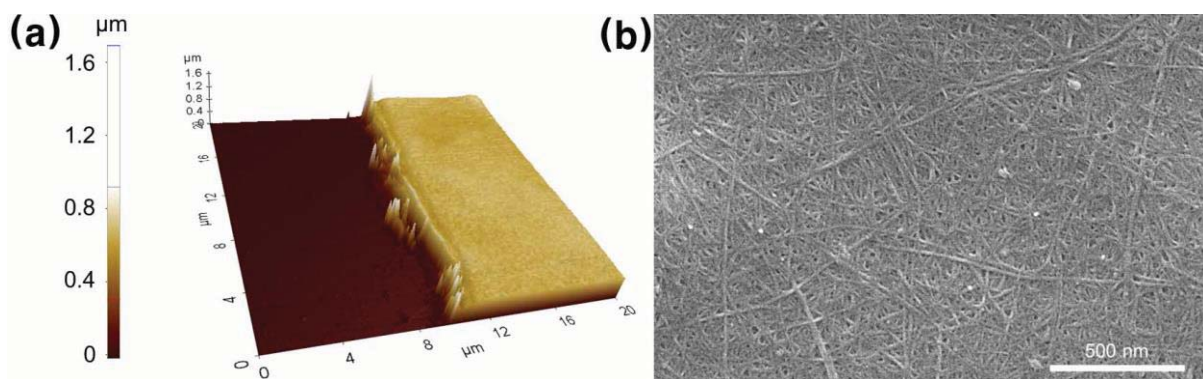


**Figure 4. (a) AFM image of a boundary between CNT film and the substrate; (b) SEM image of a CNT film. The scale bar indicates 500 nm.**

### 2.3. Experimental Apparatus and Heater Design

The CHF of DI water with bare SS316 and test heaters were measured in the apparatus as shown in Fig. 5. The apparatus consists of a horizontal flat heater submerged in water at atmospheric pressure. The bare and test heaters (Fig. 6) were  $42 \times 10 \times 2$  mm<sup>3</sup> in length, width, and thickness, respectively. The heaters were bolted to copper electrodes and heated by resistance heating using a DC power supply of 1200A-

10V capacity. The voltage and current were measured with a cDAQ system from National Instruments. The heater temperature was measured with a K-type thermocouple (TC) inserted into a small hole formed by a thin foil that was spot welded to the backside of the heater. The voltage drop across the flat heater was measured by spot welding two conductive wires into both ends of the flat heaters. The bulk temperature was measured with a K-type TC, whose sheath diameter was 1 mm and the nominal uncertainty was  $\pm 1.1$  °C as specified by the manufacturer (OMEGA Engineering).

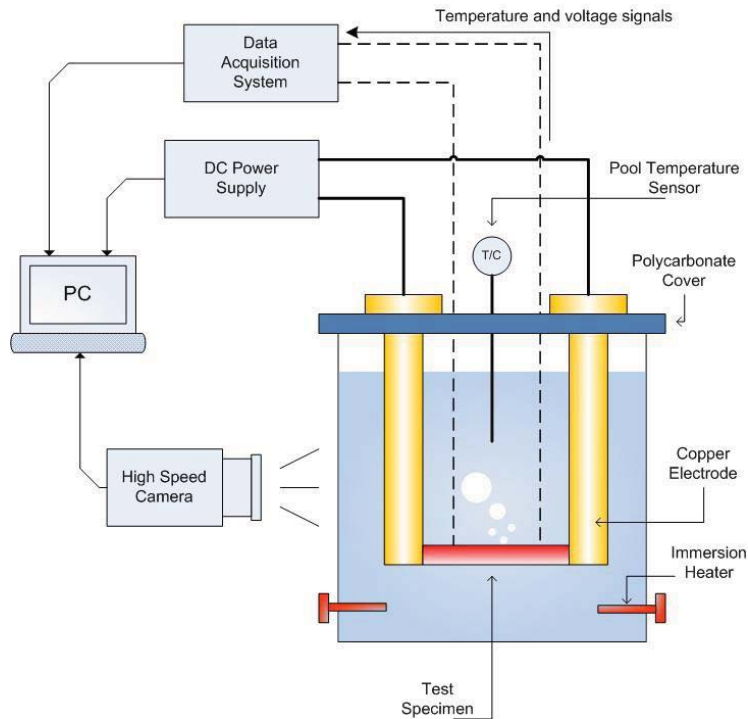


**Figure 5. Schematic of pool boiling isothermal bed apparatus.**

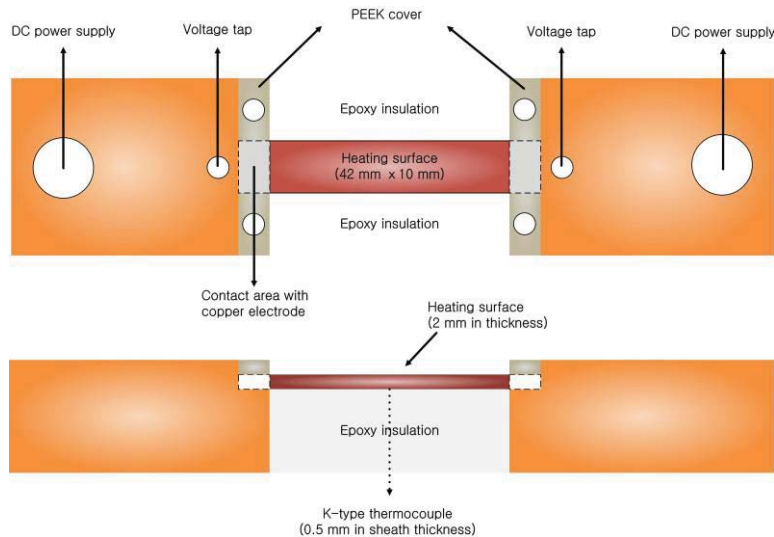


**Figure 6. Schematic of test heater assembly.**

The experimental procedure is as follows. First, the isothermal bath and water were taken to the desired temperature by the preheaters. The heaters were heated up at low flow to remove any incondensable gas bubbles sticking to the surface. After the gas was removed, the power was increased in small steps of 30 – 50 kW/m<sup>2</sup> until CHF occurred. At every heat flux increment, the wall temperature was measured simultaneously. Furthermore, a high-speed camera (Phantom V7.3) was employed to capture the bubble dynamics of evaporation/boiling at every heat flux step with a rate of 1,500 frames/sec. The experiment was terminated when CHF was detected visually and/or electrically (i.e., the wall temperature and voltage signals suddenly increased). Heat fluxes were calculated from the following equation:

$$q'' = \frac{\text{Power}}{\text{Heat transfer area}} = \frac{IV}{WL} = V^1 I^1 W^{-1} L^{-1} \quad (1)$$

The uncertainties on the current ( $U_I/I$ ), voltage ( $U_V/V$ ), and heated length ( $U_L/L$ ) and width ( $U_W/W$ ) values were less than 0.5, 0.5, 2, and 1.2 %, respectively. Eq. (3) shows the final measurement uncertainty calculation of 2.4% using a propagation of error method [10]:

$$\left(\frac{U_{q''}}{q''}\right)^2 = \left(\frac{U_V}{V}\right)^2 + \left(\frac{U_I}{I}\right)^2 + \left(\frac{U_W}{W}\right)^2 + \left(\frac{U_L}{L}\right)^2, \quad (2)$$

$$\frac{U_{q''}}{q''} = \left[ (0.005)^2 + (0.005)^2 + \left(\frac{0.2 \times 10^{-3}}{10 \times 10^{-3}}\right)^2 + \left(\frac{0.5 \times 10^{-3}}{42 \times 10^{-3}}\right)^2 \right]^{1/2} = 0.024 \quad (3)$$

### 3. RESULTS AND DISCUSSION

#### 3.1. Measurement of Surface Characteristics

The contact angle is an indicator used to quantify the surface wettability effect, which is a dominant parameter affecting the boiling heat transfer characteristics [11]. The Kandlikar's model suggests a contact angle is a major parameter, and shows the wettability effect on the CHF phenomenon [12]. Thus, a static contact angle measurement was performed to evaluate the wettability of the test heater. Figure 7 shows apparent contact angles on the heaters for each case. The resulting contact angles were estimated to be 81.6° for the bare sample, 16.4° for the Cr coated sample, and 98.8° for the CNT coated sample, respectively. After the sputtering process, the wettability of the Cr coated sample increased significantly, and a difference of 65.2° was evaluated. On the other hand, the wettability of the CNT coating on the SS316 substrate slightly decreased a difference of 17.2°. Sethi and Dhinojwala reported that the intrinsic contact angle of CNT is 167°±3°, which represents the hydrophobic surface property [13]. However, the contact angle of the CNT coating in the current measurement showed a much lower contact angle as compared to the intrinsic contact angle. It is apparent that the resulting lower contact angle was due to the existence of a porous structure by CNTs array, which was likely to enhance the capillary force. The SEM image of the CNT film also supports its porous structure as shown in Fig. 9(b).

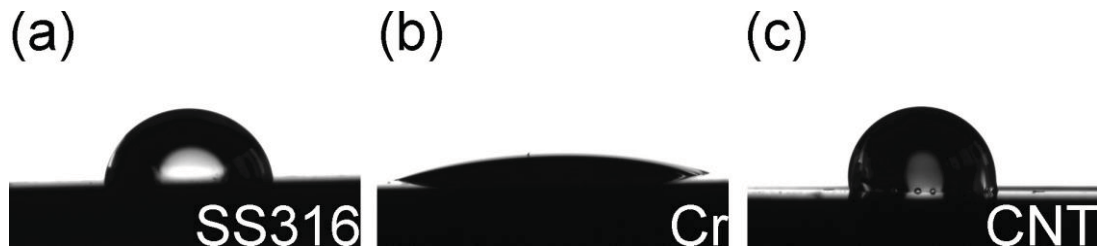


Figure 7. Apparent contact angle: (a) Bare SS316 (81.6°); (b) Cr film (16.4°); (c) CNT film (98.8°).

In addition to the wettability effect, roughness is also one of key surface parameters to affect the boiling heat transfer performance. Many studies have reported that the surface roughness is related to the surface morphology and micro-cavities, and increased boiling heat transfer was observed on a surface with higher roughness. Moreover, Ramilison et al. investigated the roughness effect on CHF, and higher CHF is expected on a rougher surface [14]. The surface roughness of the bare and coating samples was measured using AFM, and Table II summaries the measurement values. As compared to the bare sample, the roughness decreased for both the Cr and CNT coatings. Moreover, it should be noted that, although the CNT layer has the porous structure as shown in Fig. 9(b), the resulting value of roughness of the CNT layer is higher than that of the Cr layer. In vacuum filtration process described in Section 2.2, while the CNT film was formed on the Anodisc membrane, the film experienced a continuous DI water pressure at the top side of the film until the surfactants were completely removed. During this process, the film was compressed, and as a result, the CNT layer had considerably flat surface with the improved adhesion between the substrate and coating layer.

Table II. Measurement of surface characteristics

	Bare SS316	Cr	CNT
Contact Angle, °	81.6	16.4	98.8
Roughness, nm	40	21	7

Figure 8 shows a side view of Cr film deposited on the SS316 substrate. The Cr layer were uniformly and compactly developed on the substrate forming a nanoscale structure. As confirmed in the SEM image, the coating layer consists a number of Cr pillars, and a thickness of the layer was evaluated about 3.5  $\mu\text{m}$ .

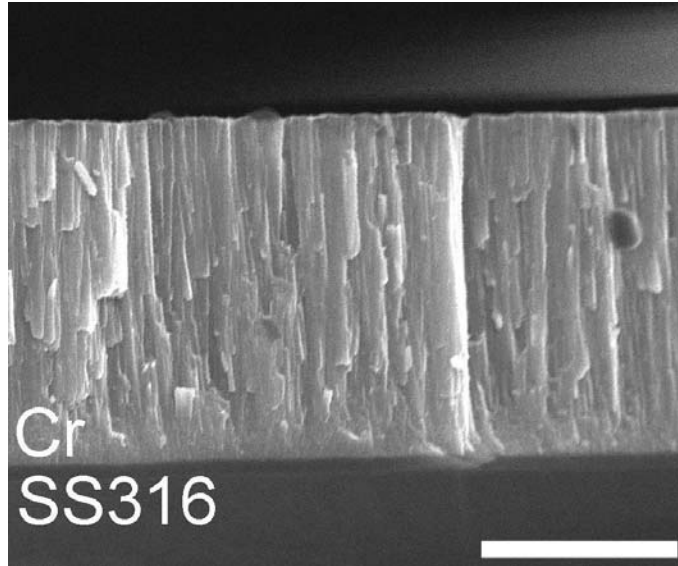


Figure 8. Side view of Cr layer on SS316 substrate. The scale bar indicates 2  $\mu\text{m}$ .

Surface morphology of the Cr and CNT films was investigated with SEM images. Figure 9 shows plain views of each coating, and different types of surface structure are observed. The Cr structure in Fig. 9(a) is compactly distributed from each other. On the other hand, the assembly of CNT wires in Fig. 9(b) forms a porous structure which may promote the liquid supply.

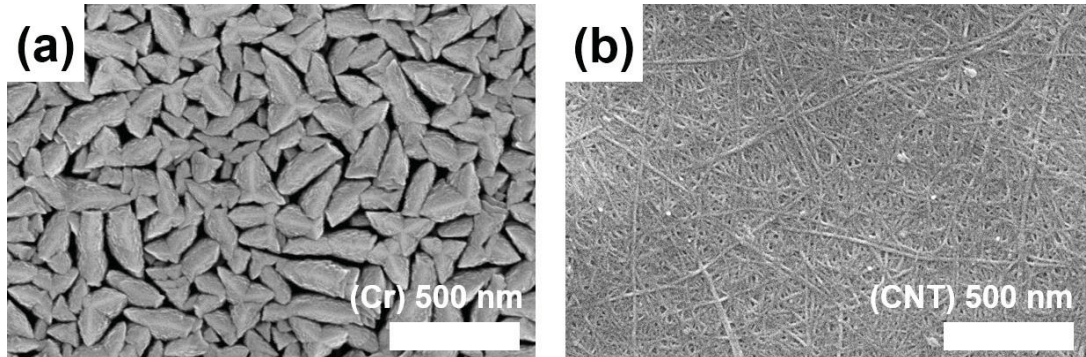


Figure 9. Plain view: (a) Cr film; (b) CNT film. The scale bar indicates 500 nm.

### 3.2. CHF of Bare and Coated Heaters

Figure 10 shows resulting CHF values in the experiment, and CHF of the bare sample is  $820 \text{ kW/m}^2$ . The obtained CHF of the bare sample was evaluated with existing models relevant to the heater conditions. The Zuber's model (1959) shown in Eq. (4) is widely adopted as a conventional CHF correlation, which was developed for an infinite flat heater [15, 16]. The Zuber's hydrodynamic limit predicts a CHF value of  $1,107 \text{ kW/m}^2$ , where  $C$  is determined by  $\pi/24=0.13$ , and this value is  $287 \text{ kW/m}^2$  larger than that of the bare sample. Chang's analysis suggests a different value of  $C$  in eq. (4). He considered the forces acting on the bubble and postulated that the CHF condition was attained when the Weber number (incorporating the velocity of liquid relative to the rising bubble) reached a critical value. The resulting CHF value on the horizontal surface as determined from Eq. (5) was approximately 75% of the vertical plate values,

with a measured CHF of 823 kW/m<sup>2</sup> [12, 17]. This value was only 3 kW/m<sup>2</sup> larger than that of the bare sample.

$$q_{crit}'' = Ch_{fg}\rho_v^{1/2} [\sigma g (\rho_l - \rho_v)]^{1/4} \quad (4)$$

$$q_{crit}'' = 0.098h_{fg}\rho_v^{1/2} [\sigma g (\rho_l - \rho_v)]^{1/4} \quad (5)$$

Although the surface characterization result indicates a notable difference of the surface wettability, the Zuber's model does not reflect the wettability effect. The Kandlikar's model (2001) shown in Eq. (6) provides a CHF prediction incorporated the effects of the surface contact angle. The Eq. (6) shows that  $\beta$  and  $\phi$  are the surface contact angle and heater orientation angle [12].

$$q_{crit}'' = h_{fg}\rho_v^{1/2} \left( \frac{1 + \cos \beta}{16} \right) \left[ \frac{2}{\pi} + \frac{\pi}{4} (1 + \cos \beta) \cos \phi \right]^{1/2} [\sigma g (\rho_l - \rho_v)]^{1/4} \quad (6)$$

As the contact angle is 16.4° for the Cr coated heater discussed in Section 3.1, the Kandlikar's prediction results in a CHF value of 1,528 kW/m<sup>2</sup>. This prediction implies the wettability effect with the increased CHF value as many studies report. However, even the surface wettability increased considerably, the test result shows no significant difference of CHF. The obtained CHF of the Cr coated heater (SPT-Cr) is 786 kW/m<sup>2</sup>, which is only 4% lower than that of the bare sample, as shown in Fig 10. O'Hanley et al. studied the effects of surface parameters, which are roughness, wettability, and porosity, and concluded that the wettability effect alone does not affect CHF. A dramatic increase of CHF was achieved on a highly wettable surface with the porous layer. In other words, the wettability effect appears with a combination of wettability and porosity [18]. The SEM images in Figs. 8 and 9(a) show the Cr pillars piled up densely and uniformly, which indicates no porous structure. Moreover, the surface roughness of the Cr coated heater greatly decreased. It is known that roughness affects the boiling heat transfer and CHF [14, 19], and is related to the number of nucleation sites and size of cavities [20]. The SEM image in Fig. 9(a) shows densely distributed nanoscale cavities and the smooth surface, which is likely to inhibit nucleate boiling. Furthermore, O'Hanley et al.'s work showed that, as compared to the bare sample, the similar CHF value was obtained for the smooth non-porous hydrophilic surface, whose conditions are relevant to the Cr-coated surface. Thus, even a significant increase of wettability was obtained after the sputtering process, no CHF enhancement was observed for the Cr-coated heater.

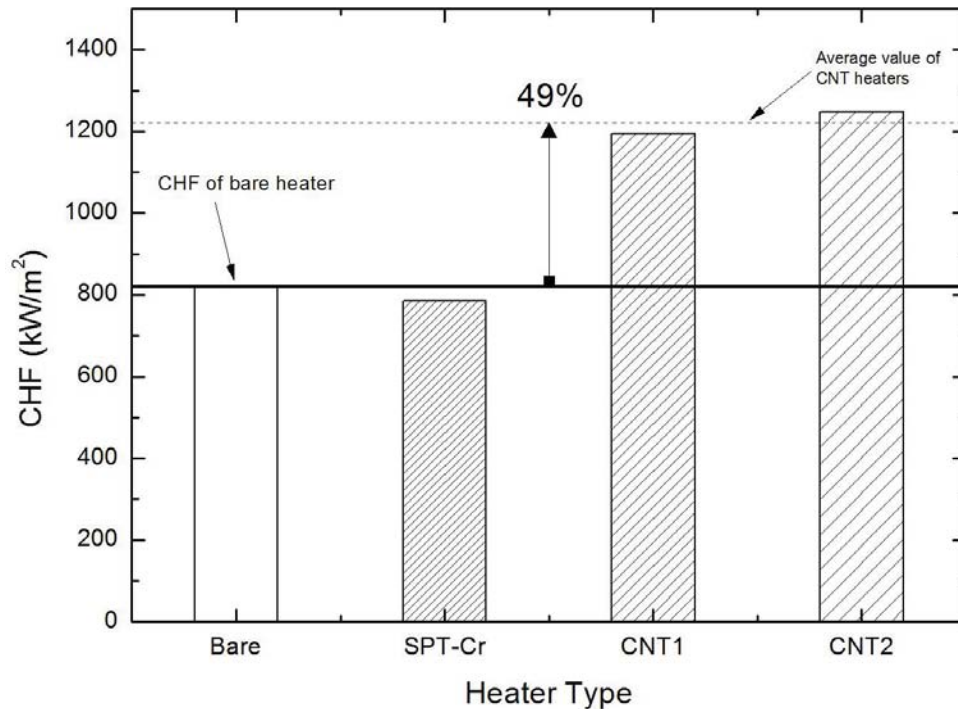


**Figure 10. CHF data of bare, Cr coated, and CNT coated heaters.**

Moreover, unlike the Cr coated sample, CHF of the CNT coated heaters (CNT1 and CNT2) increased as presented in Fig. 10 while wettability of the CNT coating slightly decreased. The obtained CHF of the CNT coated heater is 1,222 kW/m<sup>2</sup>, which is 49% higher than that of the bare sample. As shown in Fig. 9(b), the CNT arrays has the porous structure and this could give a chance to promote liquid supply, which likely resulted in increases in the capillary wicking force. As a result, the enhanced CHF was achieved for the CNT coated heater. Relevant observations were reported by Weibel and Garimella [21] and Weibel et al. [22]. In their works, an optimum CNT array could increase the permeability and result in a decrease in the capillary pressure drop, which subsequently inhibits fluid feeding. Thus, the porous structure of the CNT film significantly affects the enhanced CHF although decreases in the surface wettability and roughness were obtained.

#### 4. UMMARY AND CONCLUSIONS

In this study, Cr and CNT films were fabricated on the SS316 surface via different coating processing, which are the sputtering and vacuum filtration processes. Specifically, sophisticated surface characterization was performed with the wettability measurement and surface morphology analysis. Furthermore, the pool boiling heat transfer experiments were carried out to obtain the CHF value of the test heaters. The major findings observed from this study can be summarized as follows:

- Although a great increase in surface wettability was obtained after the sputtering process, no CHF enhancement was observed for the Cr coated heater rather the slightly decreased CHF was obtained. A similar observation was reported in the O'Hanley et al.'s work for the smooth non-porous hydrophilic surface [18].
- However, though the Cr coating heater shows the relevant surface condition to one of the O'Hanley et al.'s test, a further investigation is essentially needed to support the test result. Since the Cr and CNT layers are distinct materials, the comparison of the wettability effect on CHF is limited at the present stage.

- Unlike the case of the Cr coated heater, the surface wettability and roughness decreased slightly for the CNT coated heater. Moreover, the significantly enhanced CHF was observed for the heaters with the porous structure of CNT arrays.
- For further assessment of the coating techniques, a quantitative comparison in nucleate boiling heat transfer coefficient and visual observations are needed to investigate the boiling performance of the coated heaters.

## ACKNOWLEDGMENTS

This work was supported by the National Research Foundation of Korea (NRF) grant funded by Ministry of Science, ICT and Future Planning (MSIP) with grant number, NRF-2014M2B2A9032081.

## REFERENCES

1. S.J. Zinkle, K.A. Terrani, J.C. Gehin, L.J. Ott and L.L. Snead, "Accident tolerant fuels for LWRs: A perspective," *J. Nucl. Mater.* **448**, pp. 374-379 (2014).
2. S. Lee, K.S. Ha, H.-Y. Kim and S.J. Kim, "Validation of RCS depressurization strategy and core coolability map for independent scenarios of SBLOCA, SBO, and TLOFW," *J. Nucl. Sci. Technol.* **51**, pp. 181-195 (2013).
3. S. Seo, Y. Lee, S. Lee, H.-Y. Kim and S.J. Kim, "Effectiveness and adverse effects of reactor coolant system depressurization strategy with various severe accident management guidance entry conditions for OPR1000," *J. Nucl. Sci. Technol.* pp. 1-14 (2014).
4. J.L. Rempe, K.Y. Suh, F.B. Cheung and S.B. Kim, "In-vessel retention of molten corium: Lessons learned and outstanding issues," *Nucl. Technol.* **161**, pp. 210-267 (2008).
5. J. Buongiorno, L.W. Hu, G. Apostolakis, R. Hannink, T. Lucas and A. Chupin, "A feasibility assessment of the use of nanofluids to enhance the in-vessel retention capability in light-water reactors," *Nucl. Eng. Des.* **239**, pp. 941-948 (2009).
6. K.A. Terrani, S.J. Zinkle and L.L. Snead, "Advanced oxidation-resistant iron-based alloys for LWR fuel cladding," *J. Nucl. Mater.* **448**, pp. 420-435 (2014).
7. P. Zhao, E. Einarsson, G. Lagoudas, J. Shiomi, S. Chiashi and S. Maruyama, "Tunable separation of single-walled carbon nanotubes by dual-surfactant density gradient ultracentrifugation," *Nano Res.* **4**, pp. 623-634 (2011).
8. W. Choi and J. Hong, "Rapid Electromechanical Transduction on a Single-Walled Carbon Nanotube Film: Sensing Fast Mechanical Loading via Detection of Electrical Signal Change," *Ind. Eng. Chem. Res.* **51**, pp. 14714-14721 (2012).
9. S.B. Yang, B.S. Kong, D.H. Jung, Y.K. Baek, C.S. Han, S.K. Oh and H.T. Jung, "Recent advances in hybrids of carbon nanotube network films and nanomaterials for their potential applications as transparent conducting films," *Nanoscale* **3**, pp. 1361-1373 (2011).
10. H.W. Coleman and W.G. Steele, *Experimentation and Uncertainty Analysis for Engineers*, 2nd ed., John Wiley & Sons, New York, (1999).
11. S.J. Kim, I.C. Bang, J. Buongiorno and L.W. Hu, "Surface wettability change during pool boiling of nanofluids and its effect on critical heat flux," *Int. J. Heat Mass Transf.* **50**, pp. 4105-4116 (2007).
12. S.G. Kandlikar, "A Theoretical Model to Predict Pool Boiling CHF Incorporating Effects of Contact Angle and Orientation," *J. Heat Transf.* **123**, pp. 1071 (2001).
13. S. Sethi and A. Dhinojwala, "Superhydrophobic conductive carbon nanotube coatings for steel," *Langmuir* **25**, pp. 4311-4313 (2009).
14. J.M. Ramlison, S. P. and J.H. Lienhard, "Surface factors influencing burnout on flat heaters," *J. Heat Transf.* **114**, pp. 287-290 (1992).
15. J.G. Collier and J.R. Thome, *Convective Boiling and Condensation*, 3rd ed., Oxford University Press, Oxford, United Kingdom, (1994).

16. L.S. Tong and Y.S. Tang, *Boiling Heat Transfer and Two-Phase Flow*, 2nd ed., CRC press, New York, NY, USA, (1997).
17. Y.P. Chang, "An Analysis of the Critical Conditions and Burnout in Boiling Heat Transfer," USAEC Rep. TID-14004, Washington, DC (1961).
18. H. O'Hanley, C. Coyle, J. Buongiorno, T. McKrell, L.-W. Hu, M. Rubner and R. Cohen, "Separate effects of surface roughness, wettability, and porosity on the boiling critical heat flux," *Appl. Phys. Lett.* **103**, pp. 024102 (2013).
19. P. Sadasivan, C. Unal and R. Nelson, "Perspective - Issues in Chf Modeling - the Need for New Experiments," *J. Heat Transf.* **117**, pp. 558-567 (1995).
20. B.J. Jones, J.P. McHale and S.V. Garimella, "The Influence of Surface Roughness on Nucleate Pool Boiling Heat Transfer," *J. Heat Transf.* **131**, pp. 121009 (2009).
21. J.A. Weibel and S.V. Garimella, "Visualization of vapor formation regimes during capillary-fed boiling in sintered-powder heat pipe wicks," *Int. J. Heat Mass Transf.* **55**, pp. 3498-3510 (2012).
22. J.A. Weibel, S.S. Kim, T.S. Fisher and S.V. Garimella, "Carbon Nanotube Coatings for Enhanced Capillary-Fed Boiling from Porous Microstructures," *Nanoscale Microscale Thermophys. Eng.* **16**, pp. 1-17 (2012).